Journal of Magnetism and Magnetic Materials 498 (2020) 166208

Contents lists available at ScienceDirect

Journal of Magnetism and Magnetic Materials

journal homepage: www.elsevier.com/locate/jmmm

Research articles

Magnetic circular dichroism in the canted antiferromagnet α-Fe_2O_3: Bulk single crystal and nanocrystals

R. Ivantsov[a], O. Ivanova[a,b,*], S. Zharkov[a,b], M. Molokeev[a,b], A. Krylov[a], I. Gudim[a], I. Edelman[a]

[a] Kirensky Institute of Physics, Federal Research Center KSC SB RAS, Krasnoyarsk 660036, Russia
[b] Siberian Federal University, Krasnoyarsk 660041, Russia

ARTICLE INFO

Keywords:
Hematite
α-Fe_2O_3
Optical absorption
Magnetic circular dichroism
Ellipsometric parameters
Raman scattering
One-ion d-d transitions
Pare exciton-magnon transitions

ABSTRACT

Hematite, α-Fe_2O_3, is a canted antiferromagnet with the Neel temperature of 960 K. The Morin transition, which occurs when the temperature is lowered to ~260 K, when the magnetic moments of the sublattices become strictly antiparallel to each other and the resulting magnetic moment disappears, is a characteristic feature of this compound. Detailed investigations are presented here of the magneto-optical effects in the α-Fe_2O_3 nanoparticles in the transmitted light and in the α-Fe_2O_3 single crystal in the reflected light. Two types of magneto-optic features were revealed in the magnetic circular dichroism (MCD) spectrum. Some of them described by the Gauss line shape were associated with one-ion d-d transitions. Others were described by the S-shaped line with the inflection points corresponding to the absorption maxima. Last features were assigned to the pair exciton-magnon transitions. An exceptionally strong S-shaped line at 2.0–2.5 eV appeared to be a unique feature of α-Fe_2O_3 distinguishing it from other iron oxide compounds. The origin of the high effectiveness of the pair exciton-magnon interaction giving rise to this strong S-shaped feature in the MCD spectrum of α-Fe_2O_3 is discussed.

1. Introduction

Hematite, α-Fe_2O_3, occupies a very special place among all magnetic materials due to its extraordinary physical properties and many applications in various fields of human activity. Despite very long research history starting from ancient times, it still attracts the attention of researchers and engineers and continues to set puzzles. Start to study of the hematite magnetic properties goes back to the works of J. Kunz [1] and T. Smith [2,3], who revealed a weak magnetic moment of this mineral in spite of the antiferromagnetic spin ordering. Morin's discovery of the magnetic transition with the disappearance of the total magnetic moment at the crystal cooling lower ~260 K called later the Morin temperature, T_M [4], was an important stage in the study of the hematite magnetic properties. Shull with co-authors [5] has demonstrated with the neutron diffraction that antiferromagnetic ordered spins were directed along the trigonal *c*-axis of the rhombohedral α-Fe_2O_3 structure at temperatures below T_M. When the sample heating above T_M, spins flop to the basal *c*-plane and become canted out of exact antiparallel directions. The canting is of about several degrees. In 1957, I. Dzyaloshinskii developed the thermodynamic theory of the origin of the weak ferromagnetism in antiferromagnetic substances with a specific magnetic structure [6]. He showed this ferromagnetism to be due to the competition between the relativistic spin–lattice interaction and magnetic dipole interaction. Two years later, T. Moriya associated the microscopic mechanism of the antisymmetric exchange interaction with the spin–orbit coupling [7]. Then D. Treves and S. Alexander named this phenomenon simply as the antisymmetric exchange [8]. Now, this mechanism is mentioned frequently as the Dzyaloshinskii-Moriya interaction (e.g., [9,10]). The complicated temperature dependence of the interaction can lead to magnetic phase transitions, in particular, to the Morin transition in hematite. The Morin temperature, magnetic and other physical properties of hematite can be affected strongly by size effects, pressure, lattice strains, random or targeted impurities and so on [11–15]. This variability in the properties of hematite is one of the reasons why researchers continue to be interested in this material.

The study of the optical properties of a substance is important not only in view of possible applications, but also because the optical and, especially, magneto-optical spectroscopy provide valuable information about the structure of excited states and electronic transitions between them. As concerns α-Fe_2O_3, its very high optical density in visible and UV spectral regions did not allow the absorption measurements of bulk samples in transmitted light and most of the investigations of optical characteristics were carried out with the diffuse reflection using α-Fe_2O_3 powder, or with nanoparticles dispersed in any liquid, or with thin films. Sherman and Waite [16] analyzed the diffuse reflectance spectrum recorded in [17] for the sintered hematite pellets of the

* Corresponding author at: Kirensky Institute of Physics, Federal Research Center KSC SB RAS, Krasnoyarsk 660036, Russia.
E-mail address: osi@iph.krasn.ru (O. Ivanova).

https://doi.org/10.1016/j.jmmm.2019.166208
Received 26 July 2019; Received in revised form 21 October 2019; Accepted 25 November 2019
Available online 28 November 2019
0304-8853/

Mapico Inc. Co. (St. Louis, USA). They assigned maximum centered near 2.88 eV (430 nm, 23000 cm^{-1}) to the fundamental absorption band and a series of very weak features on the background of this absorption were ascribed to the one-ion crystal field (CF) d-d transitions in accordance with the Tanabe-Sugano diagram [18] and some of them to the pare exciton-magnon (EM) transitions in the Fe^{3+} ions.

Diffuse reflectance spectra of α-Fe_2O_3 nanoparticles were studied in Ref. [19] to reveal the finite size effect. Two lowest bands at E = 1.43 eV, E = 1.8 eV observed at a little different energies comparing to [16] were assigned to the CF, and band at E = 2.22 eV was compared with pare EM transition, analogously to [16]. Non-monotonous increase of the energy of EM transition with the nanoparticles size (d) decrease was shown, especially strong for d < 20 nm. Optical spectra of the chemically synthesized α-Fe_2O_3 nanocrystals of different size and structural modifications (hexagonal, *R3*c, and corundum) dispersed in ethanol were studied and analyzed in Ref. [20]. Identification of the optical spectra features was similar to that presented in the above cited references. Mitra with co-workers [21] and Chakrabarty and Chatterjee [22] measured optical absorption of the hematite nanocrystals of different morphology synthesized by the solvo-thermal method (for optical measurements nanocrystals were dispersed in the spectroscopic grade ethanol). They revealed the noticeable effect of the nanocrystal morphology in the absorption spectrum. At that, spectrum of the rhombohedral shape nanoparticles was very close to data of [16], and features in the spectrum were associated with the same CF transitions.

Marusak et al. studied optical absorption of the α-Fe_2O_3 thin films prepared by the radio-frequency magnetron sputtering in the region of 250–959 nm and of the very thin α-Fe_2O_3 single crystal in the region of 700–1000 nm, that is, in the region of the first CF transition $^6A_{1g} \rightarrow {}^4T_{1g}$ (^4G) [23]. In the last case they have measured for the first time the temperature behavior of the peak shape and intensity. Later, Jõgi et al. [24] have received optical absorption spectrum for hematite film of 50 nm thick deposited at 400 °C at quartz substrate using hybrid process of atomic layer deposition and pulsed chemical vapor deposition (ALD/pulsed CVD). The spectrum shape was similar to that published in [16], but spectral maxima were approximately 100 nm shifted to the higher energies.

New approach to the interpretation of the hematite optical spectrum has been suggested quite recently [25]. At variance with the above mentioned studies considering this spectrum to be due to the Fe^{3+} one-ion d-d transitions, the author of [25] worked out the many-body perturbation theory, including the effects of electron-hole interaction, that provided good agreement with absorption measurements available in literature and associated the hematite absorption spectrum mostly with the ligand-to-metal charge transfer excitations, giving rise to fairly localized excitons.

What concerns magneto-optical properties, several articles are available in literature devoted to observation of the α-Fe_2O_3 crystal domain structure with the magneto-optical Faraday or Kerr effects [26,27,28]. Besides, several authors used magnetic linear birefringence to study Morin transition in hematite [29,30,31]. Krinchik with co-authors have obtained the transvers Kerr effect spectral dependences and calculated off-diagonal components of the dielectric tensor for the α-Fe_2O_3 bulk single crystal [32,33,34]. They have revealed a series of peaks in the Kerr spectra and have underlined the role of the surface states in the formation of the magneto-optical spectra [33]. Balasubramanian with co-authors studied the magnetic field dependencies of the longitudinal Kerr Effect at 638 nm to characterized the α-Fe_2O_3 nanoparticles coated on a quartz substrate [35]. To our best knowledge, data on the hematite magneto-optical spectra in the transmitted light, that is, Faraday rotation (FR) and magnetic circular dichroism (MCD) are absent in literature. At the same time these effects are exceptionally informative for the deep understanding of an origin of the electron transitions forming optical and magneto-optical spectra of a substance. The absence of the data on these effects for hematite is due, partly, to the very high optical density of the crystal.

The present paper is aimed to comprehensive study of the magneto-optical spectra and optical characteristics of hematite using both an ensemble of nanocrystals and a bulk single crystal of this compound. MCD, FR, and optical absorption spectra were recorded in the transmitted light for the α-Fe_2O_3 nanocrystals. Ellipsometric parameters were measured in the reflected light for the α-Fe_2O_3 bulk single crystal which were used to calculate diagonal and off-diagonal components of the α-Fe_2O_3 dielectric tensor, optical constants, and MCD spectrum.

2. Material and methods

Hematite nanoparticles (α-Fe_2O_3) were synthesized by chemical deposition from a solution. Synthesis of nanoparticles was carried out at room temperature and constant stirring by dropwise adding an aqueous solution of ammonia (15 vol%) to an aqueous solution of iron (III) chloride (1 wt%). The precipitate was washed with distilled water. The α-Fe_2O_3 single-crystal was grown in the solution-melt: 79 wt% [Bi_2O_3 + 1.1Na_2O + 2.2B_2O_3] + 21 wt% Fe_2O_3 in the temperature range from 1075 to 1042 °C with a decreasing rate of 1–4 °C/day.

To characterize nanoparticles structure, the powder diffraction data for Rietveld analysis were collected at room temperature with a Bruker D8 ADVANCE powder diffractometer (Cu-Kα radiation) and linear VANTEC detector. The step size of 2θ was 0.016°, and the counting time was 5 s per step. Rietveld refinement was performed by using TOPAS 4.2 [36].

Morphology, structure and elemental composition of the nanoparticles were investigated using transmission electron microscope (TEM) JEM-2100 (JEOL Ltd.) operating at the accelerating voltage of 200 kV. Selected-area electron diffraction (SAED) was used to determine the structure of the nanoparticles.

The nanoparticles were also characterized by Raman spectroscopy. During collection of the Raman spectra, a low laser power of ~0.8 mW was used.

To carry out the MCD, FR, and optical absorption measurements, transparent composite plates containing the nanoparticles were prepared as it was described in [37]. The nanoparticles powder was mixed with dielectric transparent silicon-based glue ("Rayher" art. no. 3,338,100 80 ml) in the weight proportion 0.5:100 and measures were undertaken to obtain the homogeneous particles distribution using an ultrasonic bath. The mixture was placed between two thin glass plates spaced by wires 0.15 mm in diameter and solidified. The low magnetic powder concentration allowed us to exclude the interaction between nanoparticles.

The optical density spectra were recorded at 300 and 80 K with the laboratory made dual beam spectrometer.

MCD and FR were measured in the normal geometry: the magnetic vector and the light beam were directed normal to the samples plane. The modulation of the light wave from the right-hand to the left-hand circular polarization relatively to the magnetic field direction was used for the MCD measurements which was determined as the difference between the sample optical densities for right and left polarized waves in the spectral range of 1.2–3.2 eV in a magnetic field 1.3 T at room temperature and at 0.35 T in the temperature interval 80–300 K. The modulation of the polarization plane of the linearly polarized wave was applied when measuring FR which value was determined as a rotation of the light wave polarization plane when reversal the sample magnetization. The measurement accuracy was about 10^{-4} for MCD and 0.002 for FR, the spectral resolution was 20–50 cm^{-1} depending on the wavelength.

Spectra of the ellipsometric parameters were obtained in the light reflected from the (0 0 1) face of the bulk single crystal using the magneto-optical ellipsometer "Ellipse 1891" [38,39]. The light incidence angle was 70°, magnetic field up to 0.4 T was directed parallel to the (0 0 1) crystal plane. At that, ellipsometric parameters ψ and δ as well as their changes in the magnetic field Δψ and Δδ were measured in

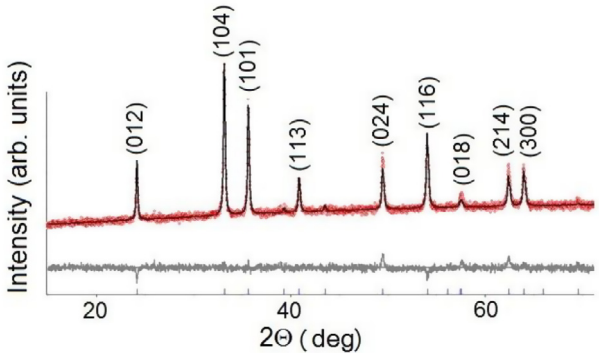

Fig. 1. The difference Rietveld plot of α-Fe_2O_3 powder sample.

the spectral region of 1.2–4.9 eV with an accuracy of 2 * 10^{-3}. Absorption and refractive indexes, k and n, as well as the real and imaginary parts of the diagonal component of the dielectric tensor were calculated according to [39]. Off-diagonal (real and imaginary parts) components and MCD were calculated using an approach suggested in [40].

3. Results and discussion

XRD spectrum of nanoparticles is shown in Fig. 1. XRD peak positions match the rhombohedral symmetry in agreement with data from literature [41,42,43]. Rietveld refinement was stable and gave low *R*-factors (R_{wp} = 1.20%, R_p = 0.91%, R_{Bragg} = 1.26%). The cell parameters were found to be a = 5.0359(4), c = 13.753(1) Å.

The TEM images of nanoparticles are presented in Fig. 2 (a). The nanoparticles are of irregular rounded shape and demonstrate the rather wide size dispersion. The average particles size was estimated as 30 nm. All interplanar distances obtained from the SAED pattern (Fig. 2 (b)) coincide with data of [44].

Raman spectra of different portions of the α-Fe_2O_3 powder are shown in Fig. 3. The close coincidence of the spectra evidences on the powder homogeneity. Six close located lines at ~218, 240, 285, 410, 487, 601 and one very strong at ~1311 cm^{-1} characteristic for hematite [45,46,47] are clearly seen in the Raman spectrum. In Ref. [45], lines at 225, 245, 291, 411, 500, 611, and 1321 cm^{-1} were observed in Raman spectra of synthetic hematite crystal. In the case of hematite nanoparticles, some of the observed lines were a little bit shifted: 225 (A_{1g}), 241 (E_g), 291 (E_g), 409 (E_g), 496 (A_{1g}) and 608 (E_g) cm^{-1} [46]

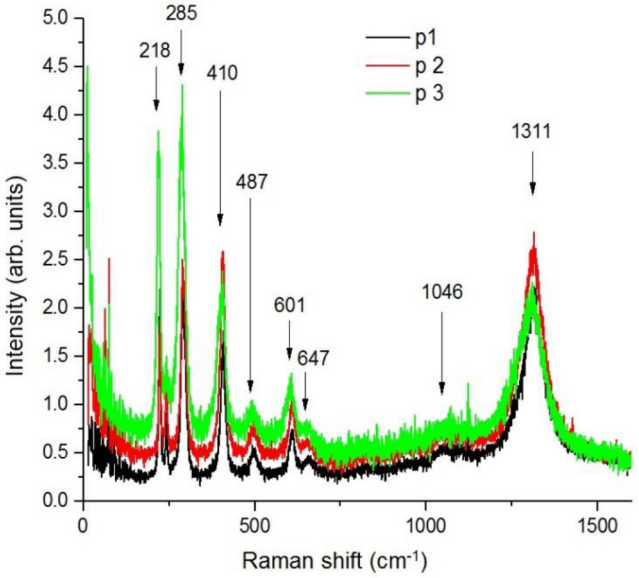

Fig. 3. Raman spectra for different portions (p1, p2, p3) of the α-Fe_2O_3 powder.

comparing to bulk crystals which is common for nanoparticles [48]. Here, symbols in brackets refer to the phonon symmetry. The additional bands between 600 and 1300 cm^{-1} might be associated with impurities analogously to [45]. The intense feature at 1311 cm^{-1} corresponds to the similar line in the Raman spectrum of the α-Fe_2O_3 powder sample observed in Ref [49] at 1320 cm^{-1} that was assigned to a two-magnon scattering arising because the exchange interaction between the neighboring antiparallel magnetized ions.

MCD spectrum of the composite sample containing α-Fe_2O_3 nanoparticles together with FR and absorption spectra recorded at room temperature are presented in Fig. 4. The values of MCD and FR were reduced to the effective thickness of hematite nanoparticles. The MCD at the maximum at 3 eV is approximately twice as small as the corresponding maximum in the MCD spectrum of yttrium-iron garnet (See Fig. 5 in [50]).

The S-shape feature in the MCD spectrum at 2.1–2.4 eV (market by vertical dashed lines in Fig. 4) corresponds to the distinct weak peak in the absorption spectrum. This feature is characteristics also for FR spectrum. Such a situation can occur in the case when two electron transitions are excited at close energies by the electromagnetic waves

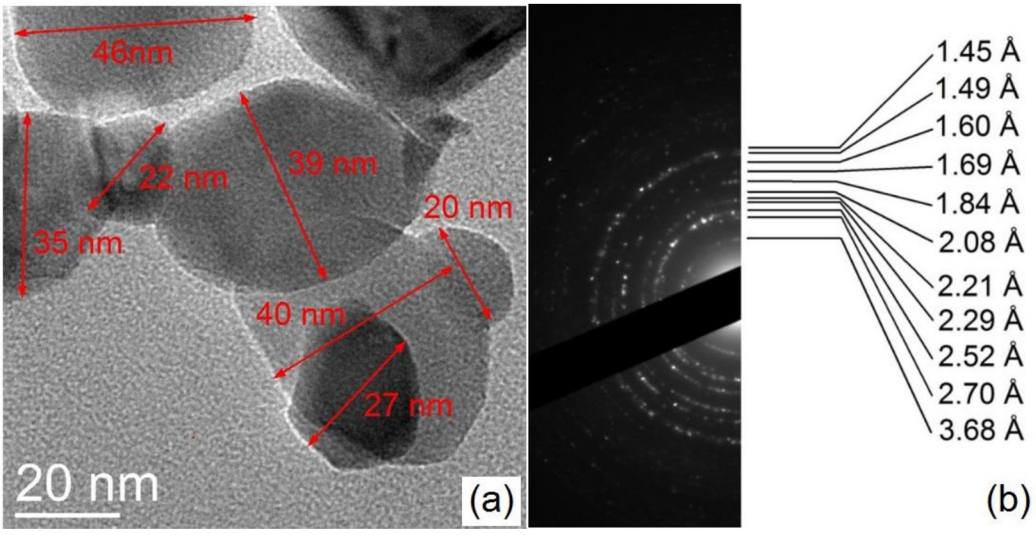

Fig. 2. TEM image of α-Fe_2O_3 nanoparticles (a) and SAED pattern with the interplanar distances (b).

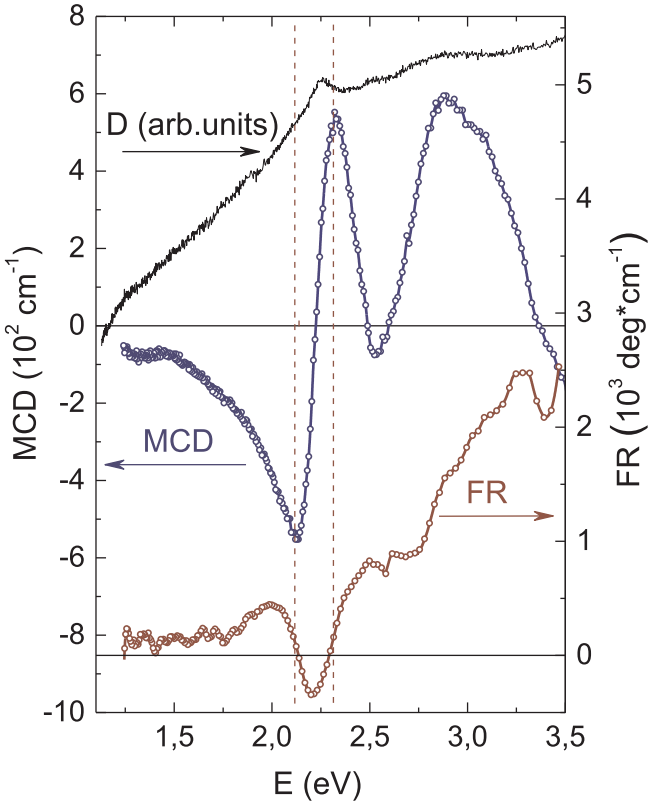

Fig. 4. The MCD, FR, and absorption spectra of α-Fe_2O_3 nanoparticles dispersed in the silicon matrix at room temperature. Magnetic field B = 1.3 T.

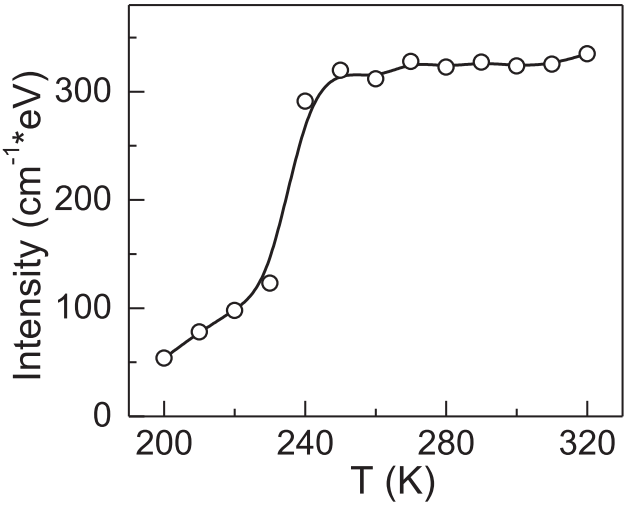

Fig. 5. The integral intensity of the MCD signal in dependence on temperature. Magnetic field B = 0.35 T. The integral intensity was determined as the sum of squares under the curve in the whole investigated spectral interval.

with the opposite circular polarizations, for example, in the case when electric dipole transitions will occur simultaneously in the neighboring exchange-coupled ions between ground and excited states accompanied by magnetic dipole transitions between sublevels of the ground state. Such a process is characteristic for the antiferromagnetic substances and it is called a pare or exciton-magnon transition [16].

Comparison is worth of MCD spectrum with spectra of ferrimagnetic compounds containing, similar to α-Fe_2O_3, only the Fe^{3+} ions – $Y_3Fe_5O_{12}$ [50] and γ-Fe_2O_3 [51] presented in literature. Two strong maxima are observed at energies 2.58 and 2.79 eV for $Y_3Fe_5O_{12}$ and at 2.3 and 2.6 eV for γ-Fe_2O_3. In the first case, the maxima are very well resolved while in the second case they are somehow overlapped. Similar two overlapping maxima are observed here for α-Fe_2O_3 at the same energy interval 2.55–3.0 eV. At energies lower 2.3 eV the MCD signal decreases sharply for both compounds γ-Fe_2O_3 and $Y_3Fe_5O_{12}$. Analogous picture was presented by Kahn, Pershan, and Remeika, who studied polar Kerr effect associated with the Fe^{3+} ions in the rare-earth orthoferrites: strong negative maximum corresponded to ~3 eV and, at the electromagnetic wave energies lower than 2.5 eV, Kerr effect signal practically disappeared [52]. Thus, it seems, that the strong S-shape signal in the interval 1.5–2.5 eV is the characteristic feature of α-Fe_2O_3.

Before comparing the magneto-optical spectra for nanoparticles with that for a single crystal, we have carried out the MCD temperature measurements for nanoparticles to reveal the Morin transition as the MCD signal is linear function of magnetization. Fig. 5 shows the decrease of the MCD signal integral intensity corresponding to the Morin transition. The transition is extended over a wider range of temperatures comparing to the literature data for α-Fe_2O_3 single crystal [4]. It starts at 260 K analogously to bulk samples and then decreases, first quickly (up to ~230 K), and then slower. At temperatures lower than 200 K, the MCD signal becomes very small to be measured correctly. Therefore, only temperature region above 200 K is shown in Fig. 5. Similar magnetization temperature changes were observed for small α-Fe_2O_3 particles in [11]. As a whole, the nanoparticles MCD temperature dependence confirms the proximity of their magnetic properties with that of the bulk hematite crystal known in literature.

The optical, magneto-optical spectra, and components of the dielectric tensor ε of the α-Fe_2O_3 single crystal were calculated from the ellipsometric parameters (ψ and δ). Tensor ε can be written as

$$\varepsilon = \begin{pmatrix} \varepsilon & ig & 0 \\ -ig & \varepsilon & 0 \\ 0 & 0 & \varepsilon \end{pmatrix} \quad (1)$$

for the samples magnetized to saturation in a magnetic field parallel to the positive z-axis direction in a right-handed set of axes. For simplicity, diagonal components were taken to be equal with each other, that is the hematite optical anisotropy and the linear magnetic birefringent were not taken into account. The right and left circular polarized components are the normal mods of the waves propagating along the positive z-axis in such a system. The real and imaginary parts of the dielectric tensor components $\varepsilon = \varepsilon' - i\varepsilon''$ and $g = g' - ig''$ are related to the complex refractive index $\eta_{\pm} = n_{\pm} - ik_{\pm}$ for the right (+) and left (−) circular polarized waves by the expression $\eta_{\pm}^2 = \varepsilon \mp g$. The ellipsometric parameter ψ is the ratio of the reflection coefficients for components of the electromagnetic wave polarized parallel and perpendicular to the light incidence plane, r_p and r_s, correspondingly, and δ is the phase shift between these components. These parameters determine the complex reflection coefficient

$$\rho = \frac{r_p}{r_s} = tg\psi e^{i\delta} \quad (2)$$

which allows determining the complex refraction index η of a medium [40]

$$\eta = sin\varphi\sqrt{1 + tg^2\varphi\left(\frac{1-\rho}{1+\rho}\right)^2} \quad (3)$$

where φ is the angle of the light incidence to a sample. Measuring ψ and δ at zero external magnetic field allows determining of diagonal components of tensor ε, refraction index n and absorption coefficient k. Measuring ψ and δ at two opposite directions of an external magnetic field, one can determine $\Delta\psi = \psi_+ - \psi_-$, and $\Delta\delta = \delta_+ - \delta_-$. Using equation for the equatorial Kerr effect [40]

$$\frac{2(\Delta\psi)}{sin2\psi} + i(\Delta\delta) = \frac{igsin2\varphi}{\varepsilon(\varepsilon cos^2\varphi - 1) + sin^2\varphi}, \quad (4)$$

we have determined g′ and g″ that were used to calculate the single

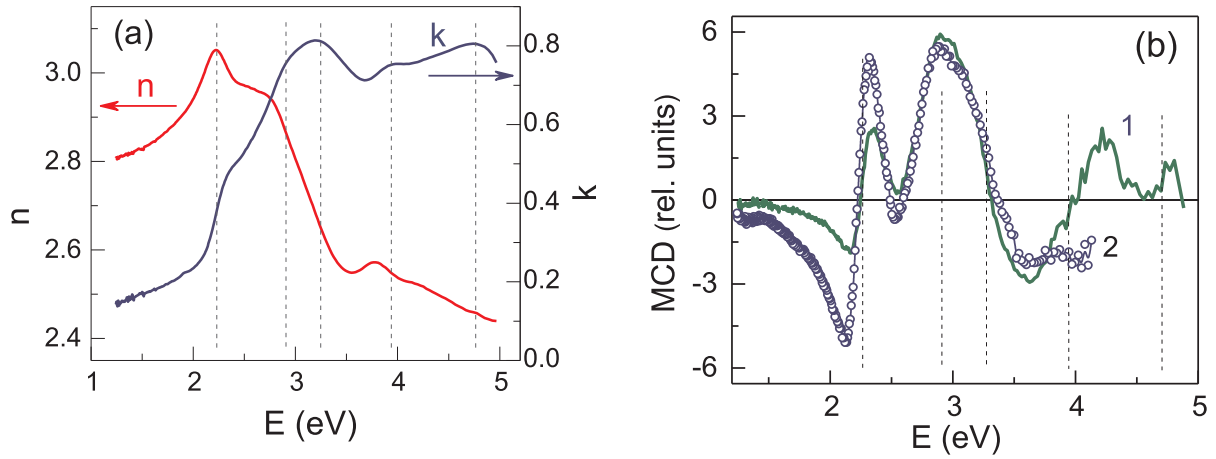

Fig. 6. (a) Spectral dependencies of the refraction index (n) and absorption coefficient (k) of the α-Fe_2O_3 single crystal, (b) MCD spectra calculated for the α-Fe_2O_3 single crystal according to Eq. (5) (curve 1) and measured directly for α-Fe_2O_3 nanoparticles (curve 2).

crystal MCD spectrum with the equation

$$\theta = \frac{4\pi}{\lambda}\left(\frac{n}{k^2+n^2}g'' - \frac{k}{k^2+n^2}g'\right). \quad (5)$$

Spectral dependencies of the refraction index (n) and absorption coefficient (k) of the α-Fe_2O_3 single crystal obtained from the measurement in zero magnetic field are presented in Fig. 6 (a). The feature positions in the single crystal k spectrum and the nanoparticles absorption spectrum (Fig. 4) are the same. Peak near 2.2 eV is more distinct in the case of nanoparticles while the peak centered at 3.2 eV is more prominent for the single crystal. Besides, the higher energy peaks at 3.9 and 4.85 eV are seen at the measurements in the reflected light. In this region nanoparticle sample is quite opaque. The redistribution of the 2.2 eV and 3.2 eV absorption peak intensities was observed for the α-Fe_2O_3 nanoparticles as their size increased from 5 to 48 nm (Fig.9 in [20]). Similar results were presented in [19]. On the other hand, absorption spectra for the α-Fe_2O_3 crystals and films available in literature [16,23] are close to the k spectrum shown in Fig. 6 (a).

Calculated spectrum for α-Fe_2O_3 single crystal is shown in Fig. 6 (b) together with the experimental MCD spectrum of α-Fe_2O_3 nanoparticles. Extrema positions in both curves are the same. Similar to the redistribution of the absorption peak intensities near 2.2 and 3.0 eV, the ratio of the MCD signals is different for these two cases. Besides, several higher energy peaks are seen in the single crystal MCD spectrum. The close coincidence of optical and magneto-optical spectra of nanoparticles and single crystal evidences that they characterized the α-Fe_2O_3 compound itself. The sample form effects in the spectra insignificantly.

As a rule, the features origin in the spectra of magnetic iron oxides is associated with several types of the electron transitions [53,16,20] one-ion CF d-d electron transitions in the Fe^{3+} ions, charge transfer transitions between Fe^{3+} ions occupying opposite sublattices, and charge transfer transitions between Fe^{3+} and ligands, charge transfer transitions between Fe^{3+} ions occupying opposite sublattices, and charge transfer transitions between Fe^{3+} and ligands.

The 1–2 eV interval was associated with d-d transitions $^6A_{1g}(^6S) \rightarrow {}^4T_{1g}(^4G)$ and $^6A_{1g}(^6S) \rightarrow {}^4T_{2g}(^4G)$ in octahedral Fe^{3+} ions. More complicated situation takes place at higher energies (2–4 eV). Here, d-d transitions from the ground to the exited states of octahedral Fe^{3+} can overlap with the transitions of other nature. As it was mentioned in the introduction, an essential contribution to absorption and magneto-optical spectra can be associated with so-called pare (exciton-magnon) transitions in the exchange-coupled Fe^{3+} ions when electric dipole transitions from the ground to the exited states and magneto dipole transitions between the ground state components splitted by magnetic field occur simultaneously in both ions. In this case, the transition energy should be approximately equal to the sum of two single ion Fe^{3+} d-d transitions [54]. From this point of view, it seems to be interesting to mention results of papers [54,55], where absorption spectra of the Fe^{3+} impurity ions substituting partly the Al^{3+} ions in Al_2O_3 crystal isostructural to α-Fe_2O_3 were investigated. When the iron concentration in Al_2O_3 crystal was very low, of about 0.1 at. %, only d-d transitions in Fe^{3+} were observed which fitted excellently to the Tanabe-Sugano diagram [18]. Increasing of the Fe^{3+} concentration up to 1 at. % led to an appearance of the additional peaks in the absorption spectrum which were ascribed to the pare transitions $2(^6A_{1g}(^6S)) \rightarrow 2({}^4T_{1g}\,({}^4G))$ at ~2.2 eV, $2(^6A_{1g}(^6S)) \rightarrow {}^4T_{1g}(^4G) + {}^4T_{2g}\,(^4G)$ near ~2.9 eV, $2(^6A_{1g}(^6S)) \rightarrow {}^4A_{1g}, {}^4E_g\,(^4G) + {}^4T_{1g}\,(^4G)$ at ~3.7 eV. At that, absorption maxima associated with the first and third transitions are rather insensitive while the second transition contribution is almost invisible. In principle, features associated with transitions of this type should be observed more clearly in α-Fe_2O_3. Indeed, the S-shape line centered at 2.2 eV observed here is so intensive that the two first d-d transitions are not seen, practically, on the background of its low energy tail.

In Ref. [56] the absorption spectrum of the thin slice of the α-Fe_2O_3 single crystal was investigated in wide temperature region. At room temperature no peaks were observed corresponding to the transitions $^6A_{1g}(^6S) \rightarrow {}^4T_{1g}(^4G)$ and $^6A_{1g}(^6S) \rightarrow {}^4T_{2g}\,(^4G)$, like to our room temperature absorption spectra. At 4.2 K two maxima centered at 1.4 and 1.9 eV were seen distinctly which can be attributed to the transitions mentioned above. Magneto-optical effects are observed in α-Fe_2O_3 only at temperatures higher than the Morin transition temperature, as it was shown above. Therefore we have carried out the decomposition of the g'' spectrum (Fig. 7) which coincides with the MCD spectrum (Fig. 6 (b)) into components of different forms. Comparing the g'' spectrum with the k spectrum (Fig. 6 (a)) shows that energies of several maxima in g'' and k spectra coincide with each other while other maxima in k spectrum correspond to the inflection points in g'' spectrum. Taking into account this circumstance, the best fit of the sum of the decomposition components to the experimental g'' curve was obtained with four Gaussian lines (E_1, E_2, E_4, E_5) and three Gaussian derivatives (E_3, E_6, E_7). At that, the E_1 and E_2 component energies coincide very close with energies of the $^6A_{1g}(^6S) \rightarrow {}^4T_{1g}(^4G)$ and $^6A_{1g}(^6S) \rightarrow {}^4T_{2g}\,(^4G)$ transitions determined in [56]. Energies corresponding to the gravity centers of the Gaussian E_1, E_2, E_4, E_5 lines match very well to the Tanabe-Sugano diagram (Fig. 8). Therefore, the corresponding maxima in the g'' curve, and consequently in the MCD curve should be attributed to the one-ion transitions between ground and excited 3d states (Table 1).

The S-shape of the MCD features at E_3, E_6, E_7 can be associated with the pare excitons-magnon mechanism of the light absorption by two neighboring exchange coupled 3d ions what takes off, partly, the forbiddance of Fe^{3+} d-d transitions.

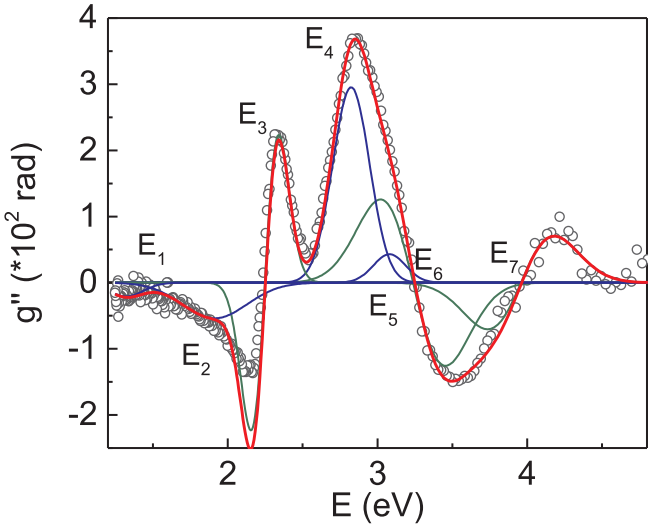

Fig. 7. The g'' spectrum decomposition to the Gaussian and Gauss derivative components. E notation shows the gravity centers of the corresponding absorption features.

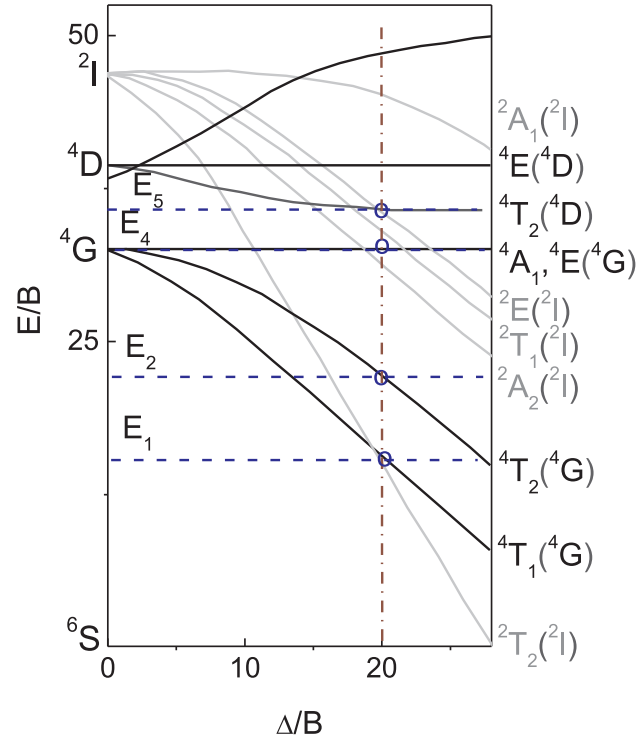

Fig. 8. Tanabe-Sugano diagram for high-spin Fe^{3+} in octahedral coordination. The state energies were calculated using the g'' spectrum decomposition.

Most intense S-shape feature at ~2.2 eV consists of two peaks of the opposite signs, with the peak-to-peak distance equal to ~1600 cm^{-1}, what is close to the energy of the two-magnon peak observed in the Raman spectrum 1311 cm^{-1} (Fig. 3). The distance between two excitons should not be equal exactly to two magnon shift in the Raman spectrum because other processes like phonons can be involved into transition. Other two transitions, which we ascribed to pare transitions too, overlap with the one-ion transitions and look not so distinct. Energies of the g'' decomposition components and their identification with crystal field transitions are presented in Table 1 in comparison with data of several authors obtained from the absorption spectra of Fe^{3+} impurities in sapphire [54] and from the diffuse reflectance spectra of α-Fe_2O_3 powder [16,22,57]. Joint optical and magneto-optical investigations led to a slightly different interpretation of the spectral features in the high-energy part of the spectrum – E_6 and E_7. However, the most interesting very intensive S-shape line at 2.2–2.3 eV is ascribed to the pare exciton-magnon transition by all authors except Piccinin [25] who has performed, as it was mentioned in the Introduction, the first principal calculations of the α-Fe_2O_3 band structure using many-body perturbation theory, including the effects of electron-hole interaction by solving the Bethe-Salpeter equation. Based on the obtained band structure, Piccinin calculated the diagonal components of the α-Fe_2O_3 dielectric function and compared the results with the experimental data on the α-Fe_2O_3 absorption spectrum [58,59]. The absorption maximum in the vicinity 2.2–2.3 eV was interpreted as the first optically allowed transition from the top of the valence band to the bottom of the conduction band. Such a transition should be of the ligand-to-metal charge transfer type because the valence band comes from a hybridization between O 2p and Fe 3d states while the conduction band is determined by the Fe 3d states.

Such an interpretation raises objections. Optical transition from the valence band to the conduction band should not be of the magneto-optical active [60], while the α-Fe_2O_3 magneto-optical activity in this spectral interval is extremely high. More than that, the width of the S-shape line (the energy distance between the maxima of the opposite signs) correlates well with the energy of the two magnon scattering in the Raman spectrum (Fig. 3). This feature distinguishes hematite from other magnetic compounds of Fe^{3+} similar to the Morin transition, which distinguishes hematite from other weak ferromagnets. Possibly, both of these features – very effective excitons-magnon interaction responsible for the S-shape line in the MCD spectrum and the Morin transition have the same origin associated with the Dzyaloshinskii-Moriya interaction, which is extremely sensitive to the crystal structure, in particular, to the local broken inversion symmetry [9,10]. Such an approach could explain the difference between the S-shape line intensity in the MCD spectra of single crystal and nanoparticles. In the second case, Fe^{3+} ions with the broken couplings in the surface nanoparticle layers can lead to the higher probability of pare excitations.

4. Conclusions

In summary, we carried out a complex investigation of optical and magneto-optical spectra in the transmitted and reflected light for two types of samples: α-Fe_2O_3 nanocrystals and a bulk single crystal. Optical absorption spectra, FR, and MCD at different temperatures were obtained for the ensemble of the nanocrystals, and parameters of the ellipse of the reflected light were obtained for the α-Fe_2O_3 single crystal both with and without external magnetic field. The ellipse parameters were used to calculate diagonal and off-diagonal components of the α-Fe_2O_3 dielectric tensor, optical constants, and MCD spectrum. The main features in the MCD spectra were shown to be close for the nanocrystals and single crystal: the feature energies were the same for both cases, but some differences in the distribution of the maximum intensities were revealed. A very strong S-shaped line in the energy interval of 2.0–2.5 eV is the main peculiarity in the MCD spectrum which distinguishes hematite from other magnetic ferric compounds. This line was ascribed to the pair exciton-magnon process when electric dipole transitions occur simultaneously in the neighboring exchange-coupled Fe^{3+} ions accompanied by the magnetic dipole transitions between the sublevels of the ground state. This statement is based on the Raman spectroscopy data obtained for nanoparticles. The electric dipole transitions were determined as $2(^6A_{1g}(^6S)) \rightarrow 2(^4T_{1g}(^4G))$ and the S-shaped line peak-to-peak distance was approximately equal to the two magnon scattering peaks in the Raman spectrum. This transition is so strong that it was detected as a weak peak on the background of the fundamental absorption by several authors. However, we have shown here this transition to have very high magneto-optical activity that allows one to disagree with the recently proposed theoretical interpretation [25] of

Table 1
Energies (eV) of the g'' decomposition components (E_1-E_7) and the components identification with CF and pare transitions comparing to the results of other authors.

	Electron transition	This research	[55]	[16]	[57]*	[22]
E_1	$^6A_{1g}(^6S) \rightarrow {}^4T_{1g}\ (^4G)$	1.4	1.17	1.4		
E_2	$^6A_{1g}(^6S) \rightarrow {}^4T_{2g}\ (^4G)$	1.92	1.78	1.91		
E_3	**$2(^6A_{1g}(^6S)) \rightarrow 2(^4T_{1g}\ (^4G))$**	2.24	–	2.34	2.21	2.18–2.23
E_4	$^6A_{1g}(^6S) \rightarrow {}^4A_{1g}, {}^4E_g\ (^4G)$	2.83	2.76	2.79	2.76	2.7–3.03
E_5	$^6A_{1g}(^6S) \rightarrow {}^4T_{2g}\ (^4D)$	3.11	3.13	3.06	3.22	
E_6	**$2(^6A_{1g}(^6S)) \rightarrow {}^4T_{1g}\ (^4G) + {}^4T_{2g}\ (^4G)$**	3.23				
	$^6A_{1g}(^6S) \rightarrow {}^4E_g\ (^4D)$		3.32	3.36	3.76	
E_7	**$2(^6A_{1g}(^6S)) \rightarrow {}^4T_{1g}\ (^4G) + {}^4A_{1g}, {}^4E_g\ (^4G)$**	3.95				
	$^6A_{1g}(^6S) \rightarrow {}^4T_{1g}\ (^4D)$		3.7	3.88		3.76–4.0
		B = 680 cm^{-1}	B = 660 cm^{-1}	B = 540 cm^{-1}		
		Dq = 1360 cm^{-1}	Dq = 1510 cm^{-1}	Dq = 1400 cm^{-1}		

* The energies of the absorption features were presented in Ref. [57] but their identification with the particular electron transitions was not made.

this peak as the first optically allowed transition from the top of the valence band to the bottom of the conduction band.

We have made an assumption on the same origin of the Morin transition and very effective pair excitons-magnon mechanism responsible for MCD associated with the peculiarities of the Dzyaloshinskii-Moriya interaction in hematite. We hope it will stimulate new theoretical studies in this region similar to that carried out for series of weak ferromagnets with different transition ions in Ref. [9,10].

Declaration of Competing Interest

The authors declare that they have no known competing financial interests or personal relationships that could have appeared to influence the work reported in this paper.

Acknowledgments

The authors thank S.L. Sukhachev for help in conducting absorption experiments and S.G. Ovchinnikov for fruitful discussions. The work is supported by Russian Academy of Sciences in the frame of the Project № 0356-2017-0030.

Appendix A. Supplementary data

Supplementary data to this article can be found online at https://doi.org/10.1016/j.jmmm.2019.166208.

References

[1] J. Kunz, Die magnetischen eigenschaften des hãmatits, Neues Jahrbuch fur Mineralogie 1 (1907) 62–88.
[2] T. Smith, The magnetic properties of hematite, Phys. Rev. 8 (1916) 721–737.
[3] T. Smith, Magnetization and hysteresis in hematite crystals, Phys. Rev. 15 (1920) 345–364.
[4] F.J. Morin, Magnetic susceptibility of a-Fe_2O_3 and a-Fe_2O_3 with added titanium, Phys. Rev. 78 (1950) 819–820, https://doi.org/10.1103/PhysRev. 78.819.2.
[5] C.G. Shull, W.A. Strauser, E.O. Wollan, Neutron diffraction by paramagnetic and antiferromagnetic substances, Phys. Rev. 83 (1951) 333–345, https://doi.org/10.1103/PhysRev. 83.333.
[6] I.E. Dzialoshinskii, Thermodynamic theory of "weak" ferromagnetism in antiferromagnetic substances, J. Exp. Theor. Phys. 32 (1957) 1547–1562 Soviet Physics JETP, 5 (1957) 1259-1272.
[7] T. Moriya, Anisotropic superexchange interaction and weak ferromagnetism, Phys. Rev. 120 (1960) 91, https://doi.org/10.1103/PhysRev. 120.91.
[8] D. Treves, S. Alexander, Observation of antisymmetric exchange interaction in Yttrium Orthoferrite, J. Appl. Phys. 33 (1962) 1133–1134, https://doi.org/10.1063/1.1728631.
[9] G. Beutier, S.P. Collins, O.V. Dimitrova, V.E. Dmitrienko, M.I. Katsnelson, Y.O. Kvashnin, A.I. Lichtenstein, V.V. Mazurenko, A.G.A. Nisbet, E.N. Ovchinnikova, D. Pincini, Band filling control of the dzyaloshinskii-moriya interaction in weakly ferromagnetic insulators, Phys. Rev. Letters 119 (2017) 167201, , https://doi.org/10.1103/PhysRevLett. 119.167201.
[10] D. Pincini, F. Fabrizi, G. Beutier, G. Nisbet, H. Elnaggar, V.E. Dmitrienko, M.I. Katsnelson, Y.O. Kvashnin, A.I. Lichtenstein, V.V. Mazurenko, E.N. Ovchinnikova, O.V. Dimitrova, S.P. Collins, Role of the orbital moment in a series of isostructural weak ferromagnets, Phys. Rev. B 98 (2018) 104424, , https://doi.org/10.1103/PhysRevB.98.104424.
[11] O. Ozdemir, D.J. Dunlop, T.S. Berquo, Morin transition in hematite: Size dependence and thermal hysteresis, Geochem. Geophys. Geosyst. 9 (2008) Q10Z01, https://doi.org/10.1029/2008GC002110.
[12] M.A. Chuev, I.N. Mishchenko, S.P. Kubrin, T.A. Lastovina, Novel Insight into the Effect of Disappearance of the Morin Transition in Hematite Nanoparticles, Pis'ma v Zh.Eksp. i Teor. Fiz, JETP Lett. 105 (2017) 668–674 105 (2017) 700-705. doi:10.1134/S0021364017110042.
[13] S.V. Ovsyannikov, N.V. Morozova, A.E. Karkin, V.V. Shchennikov, High-pressure cycling of hematite α-Fe_2O_3: Nanostructuring, in situ electronic transport, and possible charge disproportionation, Phys. Rev. B 86 (2012) 205131, , https://doi.org/10.1103/PhysRevB.86.205131.
[14] H. Zhou, C. Yuan, Z. An, Y. Yang, K. Xu, T. Yu, X. Luo, Strain-induced phase-structure of Fe_2O_3 nanoparticles, J. All. Com. 742 (2018) 7–12, https://doi.org/10.1016/j.jallcom.2018.01.286.
[15] G.M. da Costa, E. Van San, E. De Grave, R.E. Vandenberghe, V. Barron, I. Datas, Al hematites prepared by homogeneous precipitation of oxinates: material characterization and determination of the Morin temperature, Phys. Chem. Mater. 29 (2002) 122–131, https://doi.org/10.1007/s002690100201.
[16] D.M. Sherman, T.D. Waite, Electronic spectra of Fe^{3+} oxides and oxide hydroxides in the near IR to UV, Am. Mineral. 70 (1985) 1262–1269.
[17] R.G.J. Strens, B.J. Wood, Diffuse reflectance spectra and optical properties of some iron and titanium oxides and oxyhydroxides, Mineral. Mag. 43 (1979) 347–354.
[18] Y. Tanabe, T. Moriya, S. Sugano, Magnon-induced electric dipole transition moment, Phys. Rev. Lett. 15 (1965) 1023–1025, https://doi.org/10.1103/PhysRevLett. 15.1023.
[19] L. Lu, L. Li, X. Wang, G. Li, Understanding of the finite size effects on lattice vibrations and electronic transitions of nano α-Fe_2O_3, J. Phys. Chem. B 109 (2005) 17151–17156, https://doi.org/10.1021/jp052780.
[20] Y.P. He, Y.M. Miao, C.R. Li, S.Q. Wang, L. Cao, S.S. Xie, G.Z. Yang, B.S. Zou, Size and structure effect on optical transitions of iron oxide nanocrystals, Phys. Rev. B 71 (2005) 125411, , https://doi.org/10.1103/PhysRevB.71.125411.
[21] S. Mitra, S. Das, K. Mandal, S. Chaudhuri, Synthesis of a α-Fe_2O_3 nanocrystal in its different morphological attributes: growth mechanism, optical and magnetic properties, Nanotechnology 18 (2007) 275608, , https://doi.org/10.1088/0957-4484/18/27/275608.
[22] S. Chakrabarty, K. Chatterjee, Oriented growth of α-Fe_2O_3 nanocrystals with different morphology and their optical behavior, J. Cryst. Growth 381 (2013) 107–113, https://doi.org/10.1016/j.jcrysgro. 2013.07.013.
[23] L.A. Marusak, R. Messier, W.B. White, Optical absorption spectrum of hematite α-Fe_2O_3 in near IR to UV, J. Phys. Chem. Sol. 41 (1980) 981–984, https://doi.org/10.1016/0022-3697(80)90105-5.
[24] I. Jõgi, T.J. Jacobsson, M. Fondell, T. Wätjen, J.-O. Carlsson, M. Boman, T. Edvinsson, Phase formation behavior in ultrathin iron oxide, Langmuir 31 (2015) 12372–12381, https://doi.org/10.1021/acs.langmuir.5b03376.
[25] S. Piccinin, The band structure and optical absorption of hematite (alpha-Fe_2O_3): a first-principles GW-BSE study, PCCP 21 (2019) 2957–2967, https://doi.org/10.1039/c8cp07132b.
[26] H.J. Williams, R.C. Sherwood, J.P. Remeika, Magnetic domains in α-Fe_2O_3, J. Appl. Phys. 29 (1958) 1772–1773, https://doi.org/10.1063/1.1723049.
[27] E. Appel, V. Hoffmann, H.C. Soffel, Magneto-optical Kerr effect in (titano) magnetite, pyrrhotite and hematite, Phys. Earth Planet. Interiors 65 (1990) 36–42, https://doi.org/10.1016/0031-9201(90)90073-7.
[28] P. Hejda, V. Kropáeek, E. Petrovsky, T. Zelinka, J. Zatecky, Some magnetic properties of synthetic and natural hematite of different grain size, Phys. Earth Planet. Interiors 70 (1992) 261–272, https://doi.org/10.1016/0031-9201(92)90193-Y.
[29] R.V. Pisarev, I.G. Sinii, G.A. Smolenskii, Turning of magnetic sublattices and anomalies of the cotton-mouton effect in terbium iron garnet and in hematite, ZhETF Pisma 9 (1969) 294–298.
[30] G.A. Smolenskii, R.V. Pisarev, I.G. Sinii, Birefringence of light in magnetically ordered crystals, Uspehi Fizicheskih Nauk 116 (1975) 231–270, https://doi.org/10.3367/UFNr.0116.197506b.0231 Translated in Sov. Phys. Usp. 18 (1975) 410-429.
[31] I.Sh Akhmadullin, V.A. Golenishchev-Kutuzov, S.A. Migachev, M.F. Sadykov, Magnetic birefringence of light in hematite, Fizika Tverdogo Tela 44 (2002) 321–324, https://doi.org/10.1134/1.1451024 translated in Phys. Sol. St. 4 (2002)

333-337.
[32] G.S. Krinchik, A.P. Khrebtov, A.A. Askochenskii, V.E. Zubov, Surface magnetism of hematite, ZhETF Pis. 17 (1973) 466–470.
[33] G.S. Krinchik, A.P. Khrebtov, A.A. Askochenski, E.M. Speranskaya, S.A. Belyaev, Magneto-optical spectra of 3d ions in spinel ferrites and weak ferromagnets, Zh. Eksp. Teor. Fiz. 72 (1977) 699–711.
[34] V.E. Zubov, G.S. Krinchik, V.A. Lyskov, Magneto-optical properties of hematite, Zh. Eksp. Teor. Fiz. 81 (1981) 1489–1497.
[35] S. Balasubramanian, R. Panmand, G. Kumar, S.M. Mahajan, B.B. Kale, Magneto-Optic evaluation of antiferromagnetic α-Fe_2O_3 nanoparticles coated on a quartz substrate, Proc. SPIE 9758 (2016) 975800, https://doi.org/10.1117/12.2209003.
[36] Bruker AXS TOPAS V4: General profile and structure analysis software for powder diffraction data. – User's Manual. Bruker AXS, Karlsruhe, Germany. 2008.
[37] R. Ivantsov, N. Evsevskaya, S. Saikova, E. Linok, G. Yurkina, I. Edelman, Synthesis and characterization of $Dy_3Fe_5O_{12}$ nanoparticles fabricated with the anion resin exchange precipitation method, J. Mater. Sci. Eng. B 226 (2017) 171–176, https://doi.org/10.1016/j.mseb.2017.09.016.
[38] S.V. Rykhlitskii, V.A. Shvets, E.V. Spesivtsev, V.Yu. Prokop'ev, S.G. Ovchinnikov, V.N. Zabluda, N.N. Kosyrev, S.N. Varnakov, D.V. Shevtsov, Prib. Tekh. Eksp. 2 (2012) 165.
[39] O.A. Maximova, N.N. Kosyrev, S.N. Varnakov, S.A. Lyaschenko, I.A. Yakovlev, I.A. Tarasov, D.V. Shevtsov, O.M. Maximova, S.G. Ovchinnikov, In situ magneto-optical ellipsometry data analysis for films growth control, J.M.M.M. 440 (2017) 196–198, https://doi.org/10.1016/j.jmmm.2016.12.050.
[40] O.I. Bakradze, An ellipsometric method for measuring the parameters of thin magnetic films, J. Optical Technol. 72 (2005) 225–226, https://doi.org/10.1364/JOT.72.000225.
[41] J. Hua, J. Gengsheng, Hydrothermal synthesis and characterization of mono-disperse α-Fe_2O_3 nanoparticles, Mater. Lett. 63 (2009) 2725–2727, https://doi.org/10.1016/j.matlet.2009.09.054.
[42] T. Almeida, M. Fay, Y.Q. Zhu, P.D. Brown, Process map for the hydrothermal synthesis of α-Fe_2O_3 nanorods, J. Phys. Chem. C 113 (2009) 18689–18698, https://doi.org/10.1021/jp907081j.
[43] U. Mustehsin Ali, M. Tehseen, L. Ali, M. Mumtaz Ali, Stugy of uncoated and silica-coated (α-Fe_2O_3) nanoparticles, Surfaces Interfaces 13 (2018) 196–204, https://doi.org/10.1016/j.surfin.2018.09.011.
[44] Powder Diffraction File (PDF 4+, 2018): Inorganic Phases (International Center for Diffraction Data, Swarthmore, Pennsylvania, United States, 2018).
[45] M. Hanesch, Raman spectroscopy of iron oxides and (oxy)hydroxides at low laser power and possible applications in environmental magnetic studies, Geophys. J. Int. 177 (2009) 941–948, https://doi.org/10.1111/j.1365-246X.2009.04122.x GJI.
[46] L.Yu. Novoselova, Hematite nanoparticle clusters with remarkably high magnetization synthesized from water treatment waste by one-step "sharp high temperature dehydration, RSC Adv. 7 (2017) 51298–51302, https://doi.org/10.1039/C7RA09062E.
[47] A. Lassoued, B. Dkhil, A. Gadri, S. Ammar, Control of the shape and size of iron oxide (alpha-Fe_2O_3) nanoparticles synthesized through the chemical precipitation method, Results Phys. 7 (2017) 3007–3015, https://doi.org/10.1016/j.rinp.2017.07.066.
[48] I.V. Chernyshova, M.F. Hochella, A.S. Madden, Size-dependent structural transformations of hematite nanoparticles. 1. Phase transition, Phys. Chem. Chem. Phys. 9 (2007) 1736–1750, https://doi.org/10.1039/b618790k.
[49] D.L.A. de Faria, S. Venancio Silva, M.T. de Oliveira, Raman microspectroscopy of some iron oxides and oxyhydroxides, J. Raman Spectrosc.28 873È878 (1997), https://doi.org/10.1002/(SICI)1097-4555(199711)28: 11.
[50] G.B. Scott, D.E. Lacklison, H.I. Ralph, J.L. Page, Magnetic circular dichroism and Faraday rotation spectra of $Y_3Fe_5O_{12}$, Phys. Rev. B 12 (1975) 2562–2571, https://doi.org/10.1103/PhysRevB.12.2562.
[51] I. Edelman, O. Ivanova, R. Ivantsov, D. Velikanov, V. Zabluda, Y. Zubavichus, A. Veligzhanin, V. Zaikovskiy, S. Stepanov, A. Artemenko, J. Curély, J. Kliava, Magnetic nanoparticles formed in glasses co-doped with iron and larger radius elements, J. Appl. Phys. 112 (2012) 084331, , https://doi.org/10.1063/1.4759244.
[52] F.J. Kahn, P.S. Pershan, J.P. Remeika, Ultraviolet magneto-optical properties of single-crystal orthoferrites, garnets, and other ferric oxide compounds, Phys. Rev. 186 (1969) 891–918, https://doi.org/10.1103/PhysRev. 186.891.
[53] M. Lenglet, F. Hochu, Z. Simsa, Covalency of Fe^{3+}–O2-bonds and magnetic structure in mixed oxides, Mater. Res. Bull. 33 (1998) 1821–1833, https://doi.org/10.1016/S0025-5408(98)00184-6.
[54] J. Ferguson, H.J. Guggenheim, Y. Tanabe, The origins of the colours of natural yellow, blue, and green sapphires, Phys. Soc. Jpn. 21 (1966) 347.
[55] J.J. Krebs, W.G. Maisch, Exchange effects in the optical-absorption spectrum of Fe^{3+} in Al_2O_3, Phys. Rev. B 4 (1971) 757–769, https://doi.org/10.1103/PhysRevB.4.757.
[56] P. Chen, N. Lee, S. McGill, S.-W. Cheong, J.L. Musfeldt, Magnetic-field-induced color change in α-Fe_2O_3 single crystals, Phys. Rev. B 85 (2012) 174413, , https://doi.org/10.1103/PhysRevB.85.174413.
[57] A.K. Ramasami, T.N. Ravishankar, K. Sureshkumar, M.V. Reddy, B.V.R. Chowdari, T. Ramakrishnappa, G.R. Balakrishna, Synthesis, exploration of energy storage and electrochemical sensing properties of hematite nanoparticles, J. Alloy. Compd. 671 (2016) 552–559, https://doi.org/10.1016/j.jallcom.2016.02.050.
[58] C.T. Chen, B.D. Cahan, Visible and ultraviolet optical properties of single-crystal and polycrystalline hematite measured by spectroscopic ellipsometry, J. Opt. Soc. Am. 71 (1981) 932–934, https://doi.org/10.1364/JOSA.71.000932.
[59] A.I. Galuza, V.V. Eremenko, A.I. Kirichenko, Kramers-Kronig analysis of reflection spectra of hematite, Sov. Fizika tverdogo tela 21 (1979) 1125–1129.
[60] A.V. Malakhovskii, A.L. Sukhachev, A.D. Vasil'ev, A.A. Leont'ev, A.V. Kartashev, V.L. Temerov, I.A. Gudim, Nature of optical properties of $GdFe_3(BO_3)_4$ and $GdFe_{2.1}Ga_{0.9}(BO_3)_4$ crystals and other $3d^5$ antiferromagnets, Eur. Phys. J. B 85 (2012), https://doi.org/10.1140/epjb/e2012-20953-1.